frontiers | Frontiers in Materials

TYPE Original Research
PUBLISHED 02 March 2023
DOI 10.3389/fmats.2023.1108077

OPEN ACCESS

EDITED BY
Enbo Zhu,
University of California, Los Angeles,
United States

REVIEWED BY
Du Xiang,
Fudan University, China
Yingqiu Zhou,
Technical University of Denmark,
Denmark
Huifang Ma,
Nanjing Tech University, China
Bosi Peng,
University of California, Los Angeles,
United States

*CORRESPONDENCE
Baihui Zhang,
bhzhang@csu.edu.cn

SPECIALTY SECTION
This article was submitted to Semiconducting Materials and Devices, a section of the journal Frontiers in Materials

RECEIVED 25 November 2022
ACCEPTED 15 February 2023
PUBLISHED 02 March 2023

CITATION
Yang H, Zeng L, Huang Z, Zhang T, Zhang S, Zhang X, Ao Z, Lan X and Zhang B (2023), Dislocation-driven growth of WS_2/WSe_2 quantum well superlattices.
Front. Mater. 10:1108077.
doi: 10.3389/fmats.2023.1108077

Dislocation-driven growth of WS_2/WSe_2 quantum well superlattices

Hang Yang[1,2], Li Zeng[3], Ziwei Huang[4], Tian Zhang[5], Shunhui Zhang[6], Xuyang Zhang[7], Zhikang Ao[8], Xiang Lan[5] and Baihui Zhang[6]*

[1]Beijing Blue Sky Innovation for Frontier Science, Beijing, China, [2]College of Science, National University of Defense Technology, Changsha, China, [3]Department of Materials Engineering, The University of British Columbia, Vancouver, BC, Canada, [4]Hunan Provincial Key Laboratory of Two-Dimensional Materials, State Key Laboratory for Chemo/Biosensing and Chemometrics, College of Chemistry and Chemical Engineering, Hunan University, Changsha, China, [5]College of Materials Science and Engineering, Hunan University, Changsha, China, [6]College of Physics and Electronics, Central South University, Changsha, China, [7]College of Energy and Power Engineering, Changsha University of Science and Technology, Changsha, China, [8]School of Physical and Mathematical Sciences, Nanjing Tech University, Nanjing, China

The synthesis of two-dimensional lateral heterojunctions with nanoscale characteristic width and sharp interfaces remains challenging. The quantum confinement effects are still difficult to create on 2D materials since widths smaller than 5 nm are necessary for quantum confinement effects and quantum well applications. In this study, we demonstrated the growth of a sub-2-nm tungsten sulfide quantum well array in a monolayer of tungsten selenide, driven by the climb of mismatch dislocation in a heterointerface due to the lattice mismatch. Width-controllable 2D quantum well superlattices are theoretically formed by the mismatch dislocation-driven growth mechanism, according to our analysis. Thus, abundant photonic electronic properties can be obtained in 2D quantum well superlattices formed at varied lateral heterointerfaces, which will support the study of topological insulators and superconductors.

KEYWORDS

chemical vapor deposition (CVD), lateral epitaxial growth, monolayer WSe_2, 2D quantum well superlattices, misfit dislocation-driven growth

1 Introduction

Two-dimensional (2D) lateral heterojunctions and superlattices with a series of novel properties have been generated and reported recently (Geim and Grigorieva, 2013; Liu et al., 2014; Gong et al., 2015; Li et al., 2015; Zhang et al., 2017; Chen et al., 2018; Liu et al., 2019; Shi et al., 2020; Zhang et al., 2021). Available growth methods produce featured widths in the scale of hundreds of nanometers or, at best, at micrometer scale and commonly result in rough and defective interfaces with extensive chemical intermixing (Li et al., 2015; Liu et al., 2015; Zhang et al., 2017; Shi et al., 2020). Quantum wells in conventional semiconductors with their unique electronic structure and quantum confinement have important applications in quantum cascade lasers, solar cells, high-electron mobility transistors, and infrared photodetectors (Faist et al., 1994; Gudiksen et al., 2002). In a 2D system, quantum well structures may be best generated by laterally sandwiching a nanoscale strip of a 2D semiconductor between two strips of another 2D semiconductor with a different band gap. It is theoretically necessary to control the width of the 2D quantum well comparable to the de Broglie wavelength of the carrier (the sub-10-nm regime and, ideally, less than

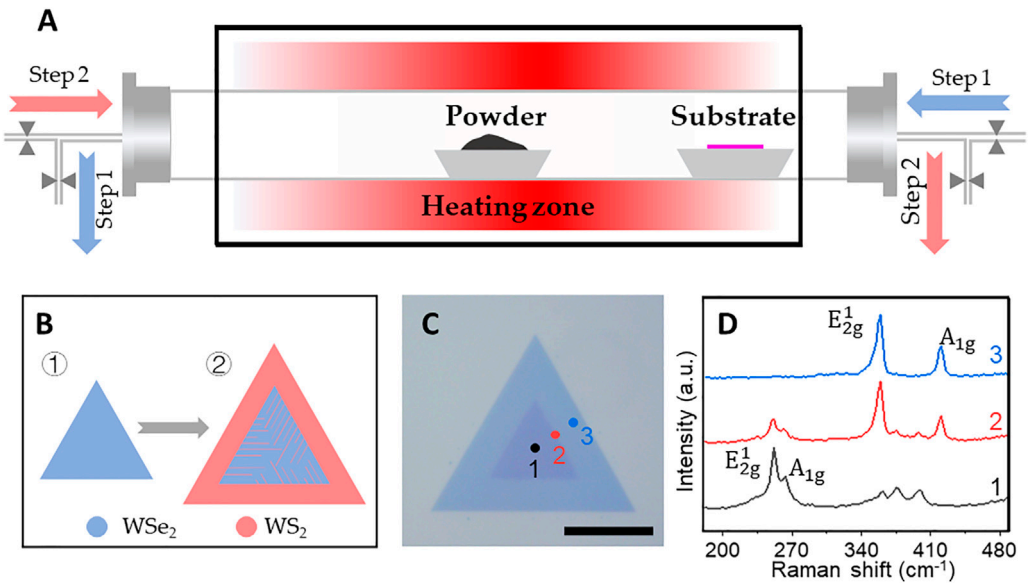

FIGURE 1
CVD synthesis strategy for monolayer WSe_2 growth and WS_2 epitaxial growth. **(A)** Diagrammatic sketch of the single supply source CVD growth method with controllable airflow directions. **(B)** Diagrammatic sketch of the WSe_2/WS_2 2D quantum well superlattice synthesis strategy. **(C)** Optical image of the WSe_2/WS_2 lateral heterojunction using the reverse airflow method; scale bar is 10 μm. **(D)** Raman spectra corresponding to the three points marked in Figure 1.

5 nm) so that quantum size effects occur. However, available growth methods only produce features with widths in the micrometer or, at best, 100 nm scale. Therefore, implementing quantum confinement effects in 2D systems remains challenging. In recent years, several studies have reported observations of quantum wells in 2D systems. Han et al. (2018) and Zhu et al. (2020) reported the fabrication methods of one-dimensional MoS_2 quantum channels in WSe_2-MoS_2 and $MoSe_2$-MoS_2 hetero-systems, respectively.

Here, we report the growth of high-quality sub-2-nm-wide quantum wells within semiconductor monolayers, making use of the lattice mismatch between two semiconducting materials in the 2D lateral heterojunctions. The growth was controlled by individual misfit dislocations formed at the lateral heterointerface between a WSe_2 and a WS_2. Atomic resolution scanning transmission electron microscopy (STEM) images revealed that these tungsten sulfide quantum wells were less than 2 nm in width and formed fully coherent lateral interfaces with the tungsten selenium monolayer matrix without extended defects.

These results showed that the insertion of metal and S atoms into the dislocation cores induced dislocation climb, with concomitant selective substitution of Se atoms around the dislocation core by S atoms. The substitution process, driven by the local strain field, led to the growth of WS_2 quantum well arrays laterally sandwiched in the WSe_2 monolayers.

Theoretically, the mismatch dislocation at the interface needed to be formed in intervals to release strain. Repetition of the misfit dislocation-driven growth mechanism formed parallel WS_2 quantum wells, and these parallel 2D narrow nano-bands were quantum well superlattices. Considering the large variety of 2D materials, 2D quantum well superlattices in varied lateral heterojunctions will display diverse photonic electronic properties; therefore, controllable width 2D quantum well superlattices are expected to be fabricated.

2 Experimental details

2.1 Growth of monolayer WSe_2

A quartz boat loaded with WSe_2 powder (~1 g) was located at the center heating zone of the furnace, as shown in Figure 1A, and a clean silica (~300 nm)/Si substrate was located at the terminal of the furnace as the growth substrate. The horizontal distance between the powder and the silicon wafer was kept between 11 and 15 cm. During the process of temperature increase, the growth substrate was placed upstream of the source, and the airflow was set to 300 sccm (along the "step 1" arrow in Figure 1A) for 15 min to remove the undesired oxygen and water from the tube. The Ar airflow was then kept at 50 sccm. When the central heating zone reached the target temperature of 1150°C, the 50 sccm airflow with the transferred direction (along the "step 2" arrow in Figure 1A) ensured the growth substrate was located downstream of the source and then maintained for 10 min for growth. Next, the airflow direction was reversed (along the "step 1" arrow in Figure 1A) to stop the growth process and allow it to naturally cool down to room temperature. The entire process occurred under ambient pressure in an argon atmosphere.

2.2 Growth of WSe_2/WS_2 2D quantum well superlattices

To obtain the WSe_2/WS_2 2D quantum well, the monolayer WSe_2 was chosen as a seed to further the epitaxial growth of the monolayer WS_2. At the same time, quantum wells started forming at the interfaces of WSe_2/WS_2 lateral heterojunctions. For the epitaxial growth of WS_2, the WS_2 powder and prepared monolayer WSe_2

(substituted for clean substrate and WSe_2 powder) were placed at the same position in another specified CVD system similar to the system used for WSe_2 growth. Likewise, during the period of temperature increase, the growth substrate was placed upstream of the source and the airflow (along the "step 1" arrow in Figure 1A) was set to 300 sccm for 15 min, and then reduced to 100 sccm and kept at that airflow rate. When the central heating zone reached the target temperature of 1120°C, the airflow was set to 100 sccm in the transferred direction (along the "step 2" arrow in Figure 1A), ensuring the growth substrate was located downstream of the source, and then maintained for 5 min for WS_2 epitaxial growth. After that, the airflow direction was reversed (along the "step 1" arrow in Figure 1A) to stop the epitaxial growth process and allow it to naturally cool down to room temperature. The entire process occurred under ambient pressure in an argon atmosphere.

2.3 Characterization

Optical microscopy and STEM were used to characterize the morphologies of the nano-heterojunctions. The Raman spectra were performed using a Renishaw confocal Raman system excited by a 488-nm laser at room temperature. The applied laser power was set to 5%, and the exposure time was approximately 0.1 s. STEM imaging and EELS analysis were carried out using a Thermo Scientific Themis Z 3.2 system equipped with a cold field-emission gun and a mirror lens corrector operating at 300 kV. All STEM experiments were completed at room temperature. The strain distribution of the nanostructure was calculated based on the geometric phase analysis method using the FRWRtools plugin for DigitalMicrograph (www.physik.hu-berlin.de/en/sem/software/software_frwrtools).

The STEM samples were prepared using a poly-methyl-methacrylate (PMMA)–assisted method. PMMA was spin-coated onto the heterojunction sample until the PMMA layer fully covered the heterojunction sample and then baked at 180°C for 3 min. Afterward, the wafer was immersed in a saturated 0.2 M NaOH solution to etch the SiO_2 layer. After the sample coated with PMMA was separated from the silicon wafer, it was transferred into fresh deionized water, repeatedly, to wash away residual contaminants and then fished by a conventional lacey carbon film TEM grid. The as-transferred sample was dried naturally in the ambient environment and then immersed in acetone overnight to clean up the PMMA coating layers. All the STEM samples were baked at 150°C for 6 h to avert unexpected contamination from hydrocarbon.

3 Results and discussion

3.1 Lateral heterojunction with 2D quantum wells

Figure 1B is the synthesis strategy diagrammatic sketch of the WSe_2/WS_2 2D quantum well, and Figure 1B① and Figure 1B② show the idealized schematic sketch of the monolayer WSe_2 and the WSe_2/WS_2 2D quantum well, respectively. The WS_2 quantum well was inserted into the monolayer WSe_2, which started to grow from the WSe_2/WS_2 interface, as depicted in Figure 1B②. The width of the quantum well in Figure 1B② is exaggerated to make the display easy to recognize and understand. Figure 1C is the optical image of the monolayer WSe_2/WS_2 lateral heterojunction synthesized on a silica/silicon substrate; it shows two concentric regions with slightly different optical contrast due to the refractive index and thickness difference between tungsten selenide and tungsten sulfide (Henrie et al., 2004; Blake et al., 2007). Here, the nanoscale WS_2 2D quantum wells formed at the WSe_2/WS_2 interface but were difficult to recognize in the optical image due to the low enlargement factor of optical microscopy. To further explore the spatial modulation of structural and optical properties in WSe_2/WS_2 lateral heterostructures, the confocal Raman microscope was used to characterize the nanostructure. We picked up three points marked "1," "2," and "3" in Figure 1C for the Raman study, where "1" (black point), "2" (red point), and "3" (blue point) are located at the internal tungsten selenium, the WSe_2/WS_2 interface, and the epitaxial tungsten sulfide area, respectively. The Raman spectra at different locations showed distinct differences: the internal region Raman spectrum had a significant peak at 250 cm^{-1} (black line in Figure 1D), consistent with the A_{1g} resonance pattern of WSe_2, and the peripheral region Raman spectrum had two significant peaks, at 350 cm^{-1} and 419 cm^{-1} (blue line in Figure 1D), corresponding to the E^1_{2g} and A_{1g} resonance patterns of WS_2. Significantly, the Raman spectrum of the WSe_2/WS_2 interface showed both the resonance modes of WSe_2 and the resonance modes of WS_2 (red line in Figure 1D), which indicate that tungsten selenium and tungsten sulfide coexist well within the same triangular domain.

3.2 Strain analysis in a WSe_2/WS_2 2D quantum well

These WS_2 quantum wells extending from the WSe_2/WS_2 interface, mostly distributed in parallel, were generally observed in the lateral WSe_2/WS_2 heterojunction samples, as shown in the STEM image in Figure 2A. Figure 2B is the enlarged view of Figure 2A, and the clear boundaries between WSe_2 and WS_2 in the WSe_2/WS_2 2D quantum well are apparent. Also, the strain distribution corresponding to Figure 2B is given in Figure 2C. The perfect lattice from the monolayer WSe_2 was used as a reference for calculating the strain. In the perfect monolayer, the lattice constant of WSe_2 was ~4% larger than that of WS_2, which indicates that the WS_2 quantum well had high and uniform tensile strain along its growth direction, leading to the observed dislocation-free transverse interface. However, the situation was different in the direction perpendicular to the growth direction, where there was a comparatively larger lattice mismatch between WS_2 and WSe_2 (~4.3 ± 0.5%), as revealed by the calculated strain distribution spectrum.

3.3 Atomic-scale sharp WS_2 2D quantum well

Figure 3A shows a 2D quantum well in which the monolayer of the WS_2 nanoribbons is laterally sandwiched between two monolayer WSe_2 nanoribbons. As shown in the STEM image in Figure 3A, the Se and S atomic sites are distinguished from the image contrast due to different atomic numbers (Krivanek et al., 2010; Zhou et al., 2012), where the WS_2 quantum well shows a lower image intensity than the surrounding monolayer WSe_2, and the WS_2/WSe_2 interface is marked by red dashed lines.

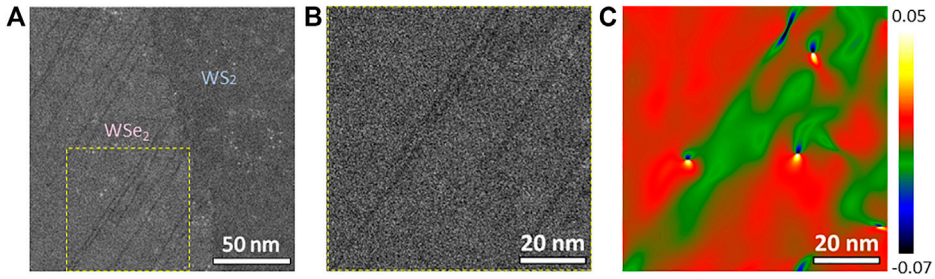

FIGURE 2
Strain analysis of WS_2 2D quantum wells at the interface between WSe_2 and WS_2. **(A)** STEM image of WS_2 quantum wells with uniform width at the WSe_2/WS_2 lateral heterojunction interface. **(B)** Enlarged view of **(A)**. **(C)** Corresponding strain distribution of **(B)**.

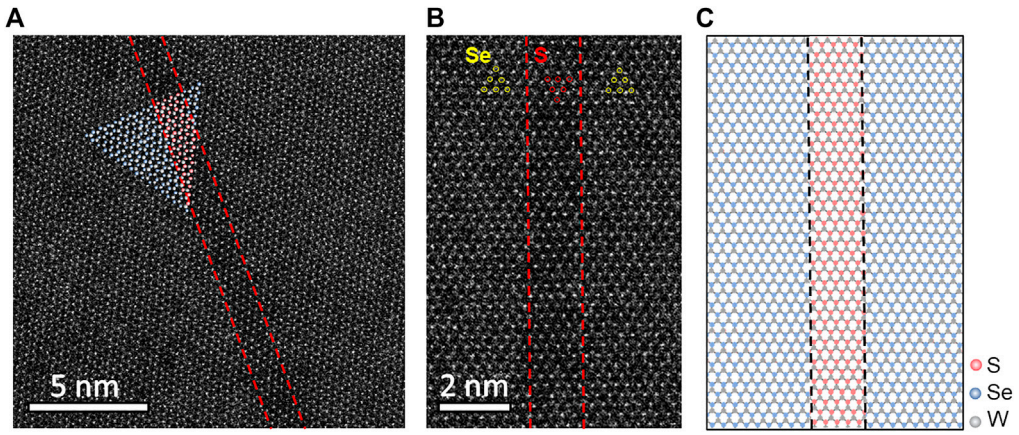

FIGURE 3
Atomic-scale sharp WS_2 2D quantum well embedded in monolayer WSe_2. **(A)** STEM image of the WSe_2/WS_2 lateral heterojunction interface; the red dashed line highlights the interface between WSe_2 and WS_2. **(B)** High-resolution STEM-ADF image of a WS_2 quantum well; the red dashed line along the armchair orientation highlights the interface between WSe_2 and WS_2. The yellow and red circles mark the Se and S atoms, respectively. **(C)** Atomic structural model of the WS_2 quantum well corresponding to **(B)**. Pink, blue, and gray spheres represent the S, Se, and W atoms, respectively.

The high-resolution STEM-annular dark-field (ADF) image of a WS_2 quantum well is shown in Figure 3B; the yellow and red circles mark Se and S atoms, respectively. It was observed that the ~1.2 nm WS_2 quantum well was embedded in a single layer of WSe_2 and growing along the hexagonal armchair orientation. Correspondingly, Figure 3C is the idealized atomic structural model of the WS_2 quantum well according to Figure 3B. The interface is highlighted by the red and black dashed lines in Figures 3B,C, respectively. It is obvious that there are no mismatches or defects at the interface, which means a fully coherent lateral interface was formed.

3.4 Formation mechanism of WS_2 quantum wells at the WSe_2/WS_2 lateral interface

Similar to film growth, strain relaxation at the epitaxial interface with intrinsic lattice mismatch produces mismatch dislocation once the critical width is exceeded (Matthews and Blakeslee, 1974; Jain et al., 1997). For the lateral WSe_2/WS_2 heterostructures, the mismatch dislocation array spaced ~8 nm in the zigzag orientation was expected to alleviate the lattice strain due to the presence of ~4% lattice mismatch between WSe_2 and WS_2. Through careful observation, it was found that WS_2 quantum wells relied on a dislocation core for growth at the lateral WSe_2/WS_2 heterointerface in general, and further growth was considered driven by misfit dislocation climb. As shown in Figure 4A, the insertion of one W atom and two S atoms from the gas source was considered initiation of the dislocation-driven growth as such dislocation drove the W and S atoms to invade the WSe_2 along the hexagonal zigzag orientation, which is consistent with our experimental results. According to statistical analysis, the width of WS_2 quantum wells is about 1.2 nm, which is equivalent to the width of the four WS_2 unit cells. A four-unit-cell-width and a one-unit-cell-width WS_2 nano-seed, shaded in light red in Figure 4B,are shown penetrating to the WSe_2 monolayer to propagate the quantum well.

Theoretically, the formation of the mismatch dislocation at the interface was required per each ~8 nm interval to release strain. After repeating the aforementioned growth mechanism, parallel WS_2 quantum wells were formed, and these parallel 2D narrow nano-bands were quantum well superlattices, as shown in Figure 4C.

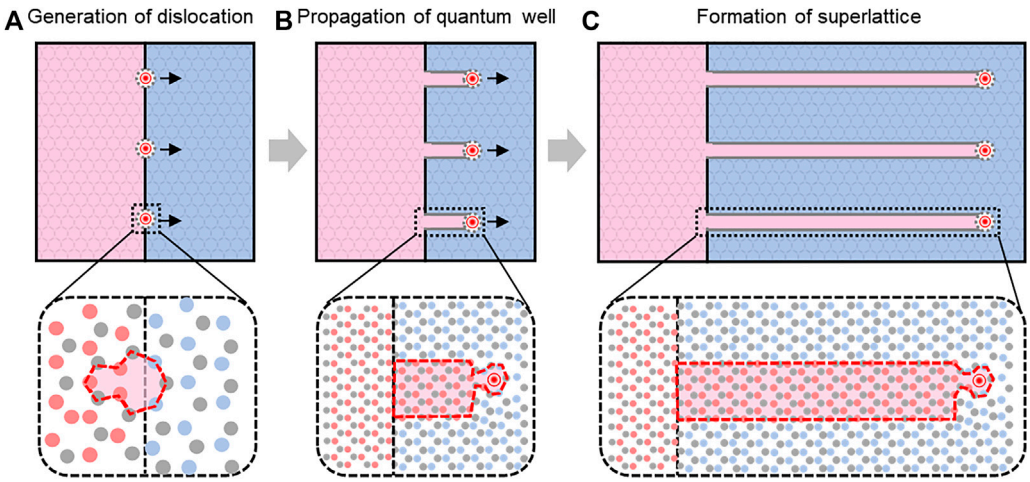

FIGURE 4
Diagrammatic sketch of the formation mechanism of WS_2 quantum wells at the interface between WSe_2 and WS_2. **(A)** Generation of dislocation. **(B)** Propagation of quantum wells. **(C)** Formation of the WS_2 superlattice.

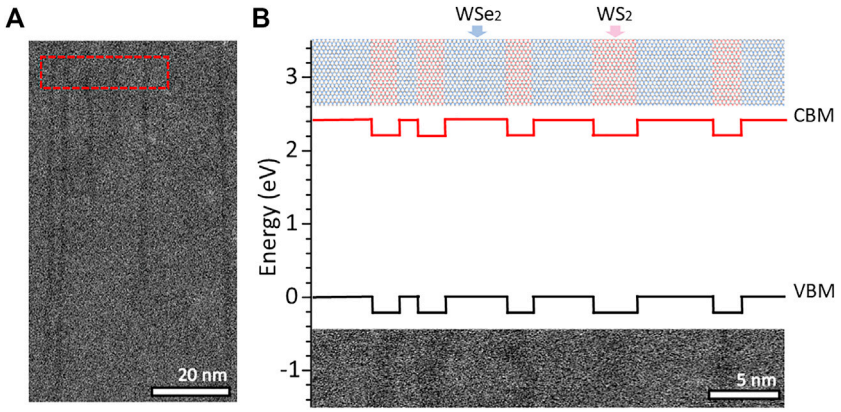

FIGURE 5
WS_2 quantum superlattice. **(A,B)** Atomic structure model of the WSe_2/WS_2 superlattice and the calculated band structure. The red and black solid lines represent the valence band maximum (VBM) and the conduction band minimum (CBM), respectively.

3.5 Promising 2D quantum well superlattices with atomically sharp lateral interfaces

According to the aforementioned results, there is potential to generate a 2D quantum superlattice, consisting of equally spaced 2D quantum wells, if growth conditions are precisely controlled. The WS_2 quantum well grown by this mechanism formed a type II band arrangement with the surrounding monolayer WSe_2, as shown in Figure 4B.

Meanwhile, the n-type doped ultranarrow WS_2 nanoribbons were expected to be conductors due to the type II band alignment. Nanoribbons of higher carrier concentrations can be obtained by this process of modulation doping as ionizing donors are distributed in the WSe_2 region and thus reduce Coulomb scattering in WS_2. Furthermore, the quantum wells shown in Figure 5A are not evenly spaced, and such a phenomenon could be attributed to the periodic array that was not initially formed at the interface. The bottom area in Figure 5B is an enlarged display of the red dotted frame in Figure 5A. There are different energy band distributions in the region of tungsten sulfide and tungsten selenide. From Figure 5A and Figure 5B, it can be concluded that the length distribution of quantum wells ranges from ten nanometers to a few microns, while the spacing between the quantum wells is about 8 nm, which is basically consistent with the previous theoretical analysis results. High-quality 2D semiconductor quantum well superlattices may be prepared by a misalignment drive mechanism if the growth parameters of the chemical vapor deposition (CVD) system are stably controlled.

4 Conclusion

To summarize, we successfully synthesized sub-2-nm quantum well arrays in WSe_2/WS_2 lateral heterojunctions. High-resolution STEM images showed the atomically sharp lateral interfaces between the

WS_2 quantum well and monolayer WSe_2. Among them, ~4% lattice mismatch between WSe_2 and WS_2 monolayers led to misfit dislocation arrays with an average spacing of 8 nm at the lateral heterointerface. After that, dislocations drove the corresponding atoms to penetrate along the hexagonal armchair orientation, which plays a key role in the efficient growth of quantum wells. According to the results of the WSe_2/WS_2 lateral heterojunction system, such quantum well superlattice structures are expected to be formed in varied lateral heterojunctions. Considering the large variety of 2D materials, 2D quantum well superlattices in varied lateral heterojunctions will display abundant photonic electronic properties, which provide new roads for the study of topological insulators and superconductors.

Data availability statement

The original contributions presented in the study are included in the article/Supplementary Material; further inquiries can be directed to the corresponding author.

Author contributions

HY: conceptualization, methodology, formal analysis, resources, visualization, and writing—original draft. LZ: methodology and formal analysis. ZH: conceptualization and visualization. TZ: methodology, and writing—review and editing. SZ: investigation, validation, and formal analysis. XZ: laboratory resources. ZA: investigation. XL: visualization. BZ: conceptualization, writing—review and editing, supervision, and project administration. All authors have read and agreed to the published version of the manuscript.

Funding

This work was supported by the Natural Science Foundation of Changsha (Grant. kq2202092).

Conflict of interest

The authors declare that the research was conducted in the absence of any commercial or financial relationships that could be construed as a potential conflict of interest.

The Reviewer, EZ, declared a shared affiliation with the author, BP, at the time of the review.

Publisher's note

All claims expressed in this article are solely those of the authors and do not necessarily represent those of their affiliated organizations, or those of the publisher, the editors, and the reviewers. Any product that may be evaluated in this article, or claim that may be made by its manufacturer, is not guaranteed or endorsed by the publisher.

Supplementary material

The Supplementary Material for this article can be found online at: https://www.frontiersin.org/articles/10.3389/fmats.2023.1108077/full#supplementary-material

References

Blake, P., Novoselov, K. S., Neto, A., Jiang, D., Yang, R., Booth, T. J., et al. (2007). Making graphene visible. *Appl. Phys. Lett.* 91, 063124. doi:10.1063/1.2768624

Chen, P., Zhang, Z., Duan, X., and Duan, X. (2018). Chemical synthesis of two-dimensional atomic crystals, heterostructures and superlattices. *Chem. Soc. Rev.* 47, 3129–3151. doi:10.1039/c7cs00887b

Faist, J., Capasso, F., Sivco, D. L., Sirtori, C., Hutchinson, A. L., and Cho, A. Y. (1994). Quantum cascade laser. *Science* 264, 553–556. doi:10.1126/science.264.5158.553

Geim, A. K., and Grigorieva, I. V. (2013). Van der Waals heterostructures. *Nature* 499, 419–425. doi:10.1038/nature12385

Gong, Y., Lei, S., Ye, G., Li, B., He, Y., Keyshar, K., et al. (2015). Two-step growth of two-dimensional $WSe_2/MoSe_2$ heterostructures. *Nano Lett.* 15, 6135–6141. doi:10.1021/acs.nanolett.5b02423

Gudiksen, M. S., Lauhon, L. J., Wang, J., Smith, D. C., and Lieber, C. M. (2002). Growth of nanowire superlattice structures for nanoscale photonics and electronics. *Nature* 415, 617–620. doi:10.1038/415617a

Han, Y., Li, M. Y., Jung, G. S., Marsalis, M. A., Qin, Z., Buehler, M. J., et al. (2018). Sub-nanometre channels embedded in two-dimensional materials. *Nat. Mater* 17, 129–133. doi:10.1038/nmat5038

Henrie, J., Spencer, K., Schultz, S. M., and Hawkins, A. (2004). Electronic color charts for dielectric films on silicon. *Opt. Express* 12, 1464–1469. doi:10.1364/opex.12.001464

Jain, S. C., Harker, A. H., and Cowley, R. A. (1997). Misfit strain and misfit dislocations in lattice mismatched epitaxial layers and other systems. *Philos. Mag. A* 75, 1461–1515. doi:10.1080/01418619708223740

Krivanek, O. L., Chisholm, M. F., Nicolosi, V., Pennycook, T. J., Corbin, G. J., Dellby, N., et al. (2010). Atom-by-atom structural and chemical analysis by annular dark-field electron microscopy. *Nature* 464, 571–574. doi:10.1038/nature08879

Li, M.-Y., Shi, Y., Cheng, C.-C., Lu, L. S., Lin, Y. C., Tang, H. L., et al. (2015). Epitaxial growth of a monolayer WSe_2-MoS_2 lateral p-n junction with an atomically sharp interface. *Science* 349, 524–528. doi:10.1126/science.aab4097

Liu, L., Park, J., Siegel, D. A., McCarty, K. F., Clark, K. W., Deng, W., et al. (2014). Heteroepitaxial growth of two-dimensional hexagonal boron nitride templated by graphene edges. *Science* 343, 163–167. doi:10.1126/science.1246137

Liu, Y., Huang, Y., and Duan, X. (2019). Van der Waals integration before and beyond two-dimensional materials. *Nature* 567, 323–333. doi:10.1038/s41586-019-1013-x

Liu, Z., Ma, L., Shi, G., Zhou, W., Gong, Y., Lei, S., et al. (2015). In-plane heterostructures of graphene and hexagonal boron nitride with controlled domain sizes. *Nat. Nanotech* 8, 119–124. doi:10.1038/nnano.2012.256

Matthews, J. W., and Blakeslee, A. E. (1974). Defects in epitaxial multilayers. I. Misfit dislocations. *J. Cryst. Growth* 27, 118–125. doi:10.1016/0022-0248(74)90424-2

Shi, E., Yuan, B., Shiring, S. B., Gao, Y., AkritiGuo, Y., et al. (2020). Two-dimensional halide perovskite lateral epitaxial heterostructures. *Nature* 580, 614–620. doi:10.1038/s41586-020-2219-7

Zhang, K., Ding, C., Pan, B., Wu, Z., Marga, A., Zhang, L., et al. (2021). Visualizing van der Waals epitaxial growth of 2D heterostructures. *Adv. Mat.* 33, 2105079. doi:10.1002/adma.202105079

Zhang, Z., Chen, P., Duan, X., Zang, K., Luo, J., and Duan, X. (2017). Robust epitaxial growth of two-dimensional heterostructures, multiheterostructures, and superlattices. *Science* 357, 788–792. doi:10.1126/science.aan6814

Zhou, W., Oxley, M. P., Lupini, A. R., Krivanek, O. L., Pennycook, S. J., and Idrobo, J.-C. (2012). Single atom microscopy. *Microsc. Microanal.* 18, 1342–1354. doi:10.1017/s1431927612013335

Zhu, C., Yu, M., Zhou, J., He, Y., Zeng, Q., Deng, Y., et al. (2020). Strain-driven growth of ultra-long two-dimensional nano-channels. *Nat. Commun.* 11, 772. doi:10.1038/s41467-020-14521-8